Biologia Futura

https://akademiai.com/loi/019

A detailed canine brain label map for neuroimaging analysis

Kálmán Czeibert[1], Attila Andics[1,2], Örs Petneházy[3,4] and Enikő Kubinyi[1]

[1]Department of Ethology, Institute of Biology, Eötvös Loránd University, Budapest, Hungary
[2]MTA-ELTE 'Lendület' Neuroethology of Communication Research Group, Hungarian Academy of Sciences – Eötvös Loránd University, Budapest, Hungary
[3]Medicopus Nonprofit Ltd., 'Kaposi Mór' Teaching Hospital, Somogy County, Kaposvár, Hungary
[4]Justanatomy Ltd., Kaposvár, Hungary

DOI: 10.1556/019.70.2019.14

Background and aims: Dogs have recently become an important model species for comparative social and cognitive neuroscience. Brain template-related label maps are essential for functional magnetic resonance imaging (fMRI) data analysis, to localize neural responses. In this study, we present a detailed, individual-based, T1-weighted MRI-based brain label map used in dog neuroimaging analysis. *Methods:* A typical, medium-headed dog (a 7.5-year-old male Golden Retriever) was selected from a cohort of 22 dogs, based on brain morphology (shape, size, and gyral pattern), to serve as the template for a label map. *Results:* Eighty-six 3-dimensional labels were created to highlight the main cortical (cerebral gyri on the lateral and medial side) and subcortical (thalamus, caudate nucleus, amygdala, and hippocampus) structures of the prosencephalon and diencephalon, and further main parts of brainstem (mesencephalon and rhombencephalon). *Discussion:* Importantly, this label map is (a) considerably more detailed than any available dog brain template; (b) it is easy to use with freeware and commercial neuroimaging software for MRI and fMRI analysis; and (c) it can be registered to other existing templates, including a recent average-based dog brain template. Using the coordinate system and label map proposed here can enhance precision and standard localization during future canine neuroimaging studies.

Original Article

Cite this article: Czeibert K, Andics A, Petneházy Ö, Kubinyi E. 2019. A detailed canine brain label map for neuroimaging analysis. *Biol. Fut. 70*, 112–120.

Received: 25 March 2019
Accepted: 28 May 2019

Keywords:
brain, template, MRI, neuroimaging, dog, label

Author for correspondence:
Kálmán Czeibert
e-mail: czeibertk@gmail.com

INTRODUCTION

Brain atlases are essential for the identification of the different brain areas during neuroscientific studies. In the field of canine science, one can distinguish macroscopic or microscopic brain atlases: the former ones usually provide cross sections from a specimen or use of macroscopic structural imaging methods [e.g., computed tomography and magnetic resonance imaging (MRI)] (Böttcher et al., 1999; Czeibert et al., 2019; Park et al., 2014; Schmidt & Kramer, 2015), whereas the microscopic approach focuses on showing the brain at histological level (Adrianov & Mering, 2010; Palazzi, 2011; Singer, 1962). During the past decades, MRI templates and label maps for different animals have been created to aid the analysis of spatially normalized neuroimaging data sets for various species, e.g., rodents (Nie et al., 2013; Schwarz et al., 2006), rabbits (Muñoz-Moreno et al., 2013), sheep (Ella & Keller, 2015; Nitzsche et al., 2015), common marmoset (Hikishima et al., 2011), dogs (Datta et al., 2012; Nitzsche et al., 2018; Tapp et al., 2006), or macaques (Adluru et al., 2012; Reveley et al., 2017; Rohlfing et al., 2012; Seidlitz et al., 2018). fMRI has become the primary mean to identify non-invasively the location of specific neuronal activities, e.g., in response to certain sensory stimuli, or in connection with some task-driven motoric activity (Cox & Savoy, 2003; Logothetis & Pfeuffer, 2004; Ulmer & Jansen, 2013). Similarities between humans and dogs regarding development, aging, and certain disorders affecting the central nervous system led researchers to a focus on the deeper understanding of the canine brain (Su et al., 1998; Adams et al., 2000; Cotman & Head, 2008; Head, 2013). Since 2009, at the Family Dog Project (FDP; https://familydogproject.elte.hu), privately owned dogs have been trained to lay motionless within an MRI scan, during awake fMRI scanning (Andics et al., 2014, 2016; Tóth et al., 2009). Awake dog fMRI is currently performed in several laboratories worldwide (Andics & Miklósi, 2018; Berns et al., 2012;

Bunford et al., 2017; Cook et al., 2015; Cuaya et al., 2016; Thompkins et al., 2016), so that it has clearly become an emerging field of comparative brain imaging. Various MRI-based canine brain templates have been developed, but the corresponding label maps either lack the level of detailedness required for an efficient fMRI analysis (Datta et al., 2012, Nitzsche et al., 2018), or they are not yet publicly available (Milne et al., 2016). Several online dog MRI brain atlases (http://vanat.cvm.umn.edu/mMRIBrain, https://www.imaios.com/en/vet-Anatomy/Dog/Dog-Brain-MRI), showing brain structures with different levels of details, are also available, but usually it is not possible to co-register them to other brain image files. Our aim was to create a detailed and easy-to-use anatomical MRI label map of the dog brain, which can be used for neuroimaging studies.

MATERIALS AND METHODS

Imaging was performed on a Philips Ingenia 3.0 T whole-body MR machine (Philips Medical Systems, Best, The Netherlands), with a Philips SENSE Flex Medium coil, using a 3D Turbo Field Echo sequence (TR = 9.85 ms, TE = 4.6 ms, with an isotropic resolution of 1 mm). Structural, T1-weighted images were obtained from 22 dogs who were trained to lay motionless during fMRI scanning (training method is described elsewhere; Andics et al., 2014) (Fig. 1). Among the 22 dogs, there were 8 Golden Retrievers, 7 Border Collies, 1 Labrador Retriever, 1 German Shepherd dog, 1 Hungarian Vizsla, 1 Cairn Terrier, 1 Spaniel, 1 Labradoodle, and 1 Chinese crested dog (aged between 1 and 12 years). None of the dogs showed behavioral problems and no neurological symptoms were present. Images were exported in Neuroimaging Informatics Technology Initiative (NIfTI) format and were evaluated with MRIcron (freeware, http://people.cas.sc.edu/rorden/mricron/index.html) and Thermo Scientific Amira for Life Sciences 6.0 software (https://www.fei.com/software). A detailed qualitative evaluation of shape, size, gyral patterns (Carreira & Ferreira, 2015a, 2015b; Evans & de Lahunta, 2012; Kawamura & Naito, 1978), and ventricular anatomy was performed by a veterinary anatomist (KC) who assessed two-dimensional NIfTI-image series and three-dimensional surface reconstructions generated from the

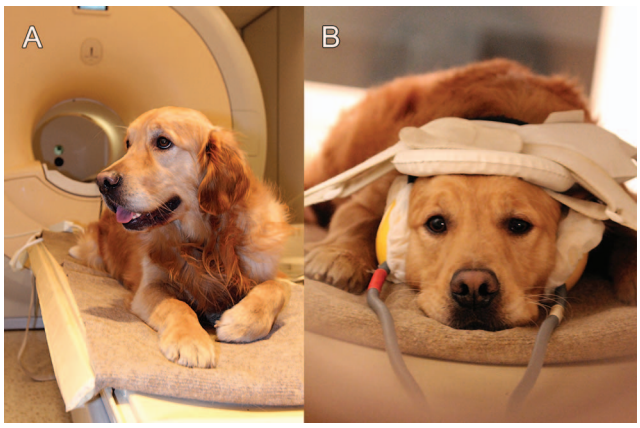

Fig. 1. A dog is participating in an awake fMRI session. Before (A) and during (B) the measurements

brain MRIs, in order to select the one individual within this sample, which showed the most typical mesaticephalic brain conformation (Hussein et al., 2012; Milne et al., 2016) with no apparent structural disorders or unusual anatomical variations. After this analysis, the brain of a 7.5-year-old male Golden Retriever was chosen as a template for labeling.

In order to have a higher resolution from this individual brain, another MRI scanning was performed on the selected dog (using the same Philips Ingenia 3T MR machine, with T1-weighted structural imaging, $0.45 \times 0.45 \times 0.5$ mm voxel size and 352 transverse slices) still in an awake state. The image volume was imported to Amira. First, the main axes were set. The horizontal (longitudinal) axis was defined as the line connecting the rostral and caudal commissures, where the zero coordinate was aligned with the rostral commissure (similarly to the Montreal Neurological Institute's MNI-coordinate system). The vertical axis was identified with the midsagittal plane. Based on these axes, the transverse, sagittal, and dorsal planes were set. Next, the volume was resampled and the field-of-view was specified, so that it would contain the neurocranium and the adjacent tissues. Finally, the origo was set to the commissura rostralis with SPM12 module (Reorient images/ Set origin to Xhairs) of Matlab (https://www.fil.ion.ucl.ac.uk/spm/software/spm12/) (Fig. 2A–C), and a three-dimensional surface model of the brain was generated with Amira (Fig. 2D–I).

Individual labels were created to highlight the main gyri and the area of the individual brain template. Labels were made with ITK Snap (http://www.itksnap.org), defining 86 different masks with the "Label Editor," distinguishing between the left and right sides in the case of symmetrical structures (Table 1). Segmentation was performed manually, by checking and refining the result in the three main orthogonal planes. The final label file was exported in NIfTI-format and two look-up-table (lut) files were created as a support to the MRIcron visualization (available on Figshare, see "Data Accessibility" statement). The anatomical terms used here comply with those in recent anatomy textbooks (Constantinescu & Schaller, 2011; Evans & de Lahunta, 2012; Nickel et al., 2003).

Our individual dog brain template was also compared to an average-based template that was recently published (Nitzsche et al., 2018), in order to check the correspondence of the individually selected brain template to the averaged one. As the latter template was created with averaging 16 dog brains and using T2-weighted imaging, and our individual template was obtained from one dog with T1-weighted imaging, the contrast (smoothed vs. sharp) and the imaging modalities (T2-weighted vs. T1-weighted) were different. Thus, a computer-paired visual matching procedure was used to decide whether the main gyri and sulci of the individual-based and the average-based template have the same location. The first phase of the assessment was to use the average-based template as the primary data set in Amira and set the individual template as the overlay data in the software's Multiplanar viewer tab. Afterward, the overlay volume was registered to the primary data set. Registration steps included rigid and non-rigid transformations. The rigid transformations were rotation and translation, and the non-rigid transformations were isoscaling, anisoscaling, and shearing.

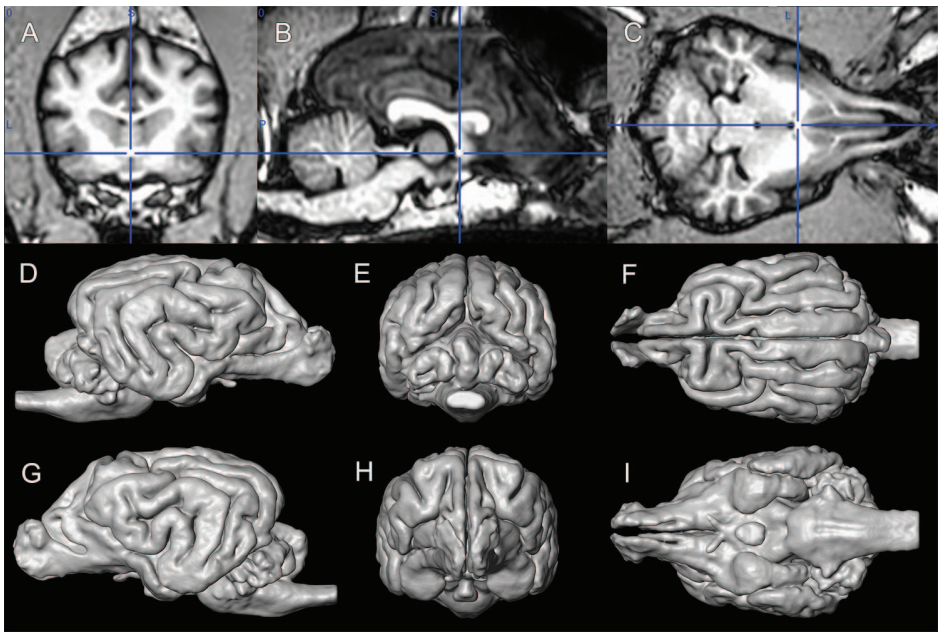

Fig. 2. The template brain in the MRIcron with crosshair positioned in the origin of the coordinate system, at the rostral commissure (A–C), and the three-dimensional reconstructions (D–I). (A) Transverse plane. (B) Midsagittal plane. (C) Dorsal plane. (D) Right lateral view. (E) Caudal view. (F) Dorsal view. (G) Left lateral view. (H) Rostral view. (I) Ventral view

These transformations are integrated check box options of the Amira software (without further settings or possibility to check the degree of freedom or their parameters); thus, all of them have been left as marked by default. The cost function used during the registration was "Correlation" (and as a control, a "Normalized Mutual Information" registration has also been performed on the same data set to see whether it makes any difference, but overlaying the two result files showed no disparity). Fitting was initially evaluated in the Multiplanar viewer of the software (Fig. 3).

During the second phase of the assessment, an "Edit New Label Field" module was added to both of the volumes and in the Segmentation Editor cerebrospinal fluid-filled spaces, of the average-based brain template, extending into the sulci were selected; on the individual brain, the surface contour of the brain was followed during segmentation. Using the "Generate Surface" module, surface reconstructions from the selected label fields were created. Non-quantitative assessment of the two co-registered fields was also created to check their post-normalization alignment.

RESULTS

An individual-based dog brain template was chosen and 86 labels were created to highlight the major cortical and subcortical structures, listed in Table 1, and shown in Figs 4 and 5. Template and label files are available on Figshare (see "Data Accessibility" statement). Labels included all the cerebral gyri both on the lateral and medial sides, the major subcortical structures (e.g., thalamus, caudate nucleus, amygdala, and hippocampus), and the main parts of the brainstem (diencephalon, mesencephalon, pons, and medulla oblongata). The label "encephalon" was used to cover most of the parts of the white matter (e.g., centrum semiovale and capsula interna) and over those regions where the subcortical nuclei could not be reliably distinguished on the image (e.g., claustrum, putamen, globus pallidus, etc.), and this was also the reason why a separate white matter mask was not created. In the case of the cerebellum, the vermis and the two hemispheres were labeled separately. The boundaries between the rostral, middle, and caudal parts of a gyrus (as in the case of the suprasylvian and ectosylvian gyri) were drawn based on subjective decision (by the author KC) regarding the inclination of the gyral arch, the surface impression of the major blood vessels originating from the middle cerebral artery, and extending from the pseudosylvian fissure to the caudodorsal and the rostrodorsal directions. The diencephalo-mesencephalic border was marked behind the line connecting the mammillary bodies to the caudal commissure. Mesencephalo-pontine and pontomedullary transitions were marked before and behind the location of the visible ventral pontine elevation (at the site of the transverse pontine fibers). Cerebral gyri were selected to comprise both the gray and the white matter of a gyrus, extending to the deepest point of the adjacent sulci. Since there are no clearly established borders on the medial frontal area by grooves, and sulci on the medio-frontal area tend to be inconsistent in their appearance, the gyrus precruciatus, gyrus frontalis, the rostral part of gyrus cinguli, and the gyrus genualis were highlighted based on subjective assessment (by the author KC).

The surface reconstruction of the average-based template (Nitzsche et al., 2018) and the individual-based template shows the sulci and the gyri of the two brain templates, respectively (Fig. 6). When the 2 three-dimensional models were co-registered, different sulci (or subarachnoid spaces) of the average-based template were visible in the corresponding locations where the sulci of the individual-based template were located (certainly, individual differences in the length of sulci were present). We focused on checking the location of the specific sulci that define the main gyri of the brain,

Table 1. Labeled structures on the individual template file, indicating the number (N), color (C) according to the lut file, and region

N	C	Region
1		Encephalon
2		Gyrus frontalis L
3		Gyrus frontalis R
4		Gyrus proreus L
5		Gyrus proreus R
6		Gyrus compositus rostralis L
7		Gyrus compositus rostralis R
8		Gyrus precruciatus L
9		Gyrus precruciatus R
10		Gyrus postcruciatus L
11		Gyrus postcruciatus R
12		Gyrus marginalis L
13		Gyrus marginalis R
14		Gyrus ectomarginalis L
15		Gyrus ectomarginalis R
16		Gyrus occipitalis L
17		Gyrus occipitalis R
18		Gyrus suprasylvius rostralis L
19		Gyrus suprasylvius rostralis R
20		Gyrus suprasylvius medius L
21		Gyrus suprasylvius medius R
22		Gyrus suprasylvius caudalis L
23		Gyrus suprasylvius caudalis R
24		Gyrus ectosylvius rostralis L
25		Gyrus ectosylvius rostralis R
26		Gyrus ectosylvius medius L
27		Gyrus ectosylvius medius R
28		Gyrus ectosylvius caudalis L
29		Gyrus ectosylvius caudalis R
30		Gyrus sylvius rostralis L
31		Gyrus sylvius rostralis R
32		Gyrus sylvius caudalis L
33		Gyrus sylvius caudalis R
34		Gyrus compositus caudalis L
35		Gyrus compositus caudalis R
36		Gyrus rectus L
37		Gyrus rectus R
38		Gyrus genualis L
39		Gyrus genualis R
40		Area subcallosa L
41		Area subcallosa R
42		Gyrus cinguli L
43		Gyrus cinguli R
44		Gyrus presplenialis L
45		Gyrus presplenialis R
46		Gyrus splenialis L
47		Gyrus splenialis R
48		Gyrus parahippocampalis L
49		Gyrus parahippocampalis R
50		Hippocampus L
51		Hippocampus R
52		Lobus piriformis L
53		Lobus piriformis R
54		Tuberculum olfactorium L
55		Tuberculum olfactorium R
56		Gyrus diagonalis L
57		Gyrus diagonalis R
58		Gyrus paraterminalis L
59		Gyrus paraterminalis R
60		Gyrus olfactorius lateralis L
61		Gyrus olfactorius lateralis R
62		Thalamus L
63		Thalamus R
64		Bulbus olfactorius L
65		Bulbus olfactorius R
66		Nucleus caudatus L
67		Nucleus caudatus R
68		Insular cortex L
69		Insular cortex R
70		Hypophysis
71		Vermis cerebelli
72		Pontine region
73		Medulla oblongata
74		Medulla spinalis
75		Mesencephalon
76		Diencephalon
77		Nervus opticus
78		Hemispherium cerebelli L
79		Hemispherium cerebelli R
80		Commissura rostralis
81		Pedunculus olfactorius L
82		Pedunculus olfactorius R
83		Area septalis L
84		Area septalis R
85		Amygdala L
86		Amygdala R

Note. L/R implies that a separate left (L) and a right (R) label file was created for a structure.

namely: fissura pseudosylvia, fissura longitudinalis cerebri, sulcus ectosylvius (rostral, middle, and caudal parts), sulcus suprasylvius (rostral, middle, and caudal parts), sulcus cruciatus, sulcus coronalis, sulcus marginalis, sulcus ectomarginalis, and sulcus presylvius. Visual inspection of the overlapping three-dimensional models clearly suggests that the individual template brain sufficiently matches the average-based template created by Nitzsche et al. (2018), that is, we could not identify any multivoxel clusters that belonged to different anatomical structures in the two templates after co-registration.

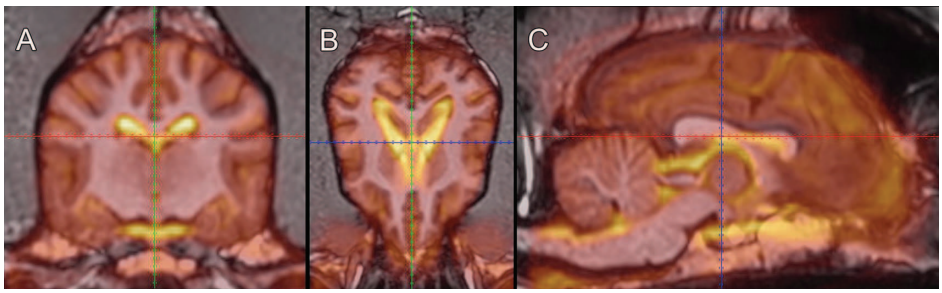

Fig. 3. Co-registering the individual (grayscaled, T1-weighted) and the average-based (yellow–orange, T2-weighted) brain templates. (A) Transverse plane. (B) Dorsal plane. (C) Sagittal plane

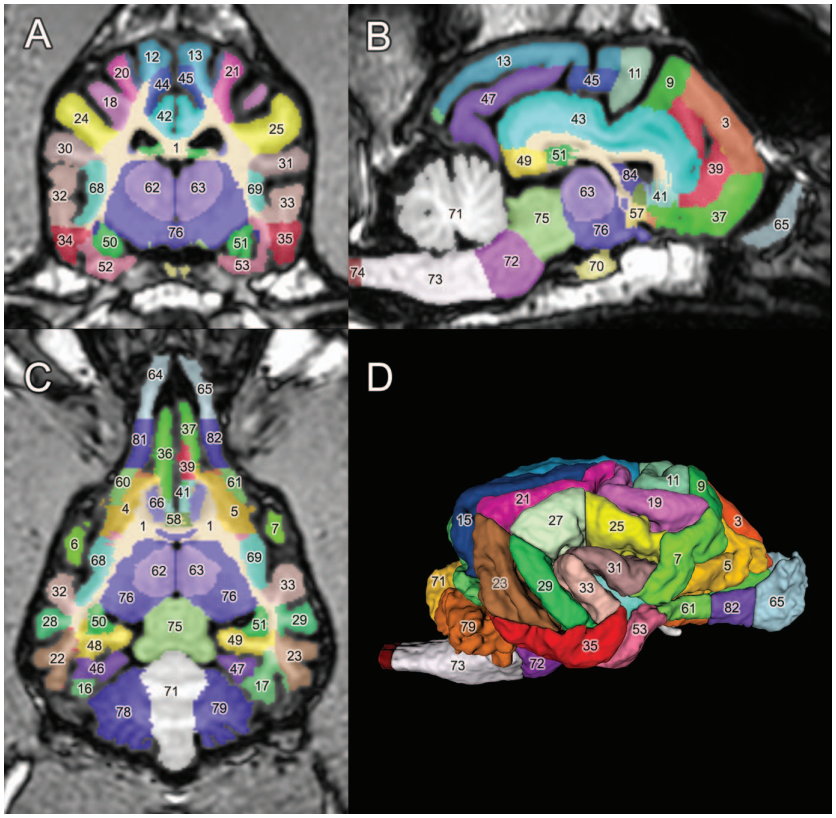

Fig. 4. Overlaying the labels on the individual template with 50% opacity (for reference of the numbers, see Table 1). (A) Transverse plane. (B) Sagittal plane. (C) Dorsal plane. (D) Three-dimensional surface view of the labels from the right lateral aspect

DISCUSSION

In this study, we presented an individual-based MRI label map for the identification of macroscopic anatomical structures of the canine brain. This individual-based label map has been developed in order to support the analysis and interpretation of fMRI studies at the FDP (Department of Ethology, Eötvös Loránd University, Budapest). The main features of this brain template are the following: (a) it provides a more detailed labeling, with marking 86 labels representing cortical and subcortical structures [compared to 39 labels (Datta et al., 2012), 5 labels (Milne et al., 2016), and 26 labels (Nitzsche et al., 2018)]; (b) co-registration to the latest published average-based template (Nitzsche et al., 2018) proved that the localization of the gyri is almost exactly overlapping between the two volumes and thus the region identified with the individual-based label map will very likely be associated to the same area on the average-based brain map; (c) it is compatible with freeware and commercial neuroimaging software packages (e.g., MRIcron, MRIcroGL, ITK Snap); (d) it defines a coordinate system similar to the Talairach and MNI templates where label identifiers can be instantly read when the crosshair is set to a given point within the brain, also with an additional fMRI data overlay. It should be taken into consideration that the template is derived only from one individual dog, contrary to other studies that used average-based templates from different breeds (Datta et al., 2012; Nitzsche et al., 2018) or average-based templates were created based on the different brain types (Milne et al., 2016). Nevertheless, a comparison between our individual-based label map and an average-based data set (Nitzsche et al., 2018) demonstrated a good

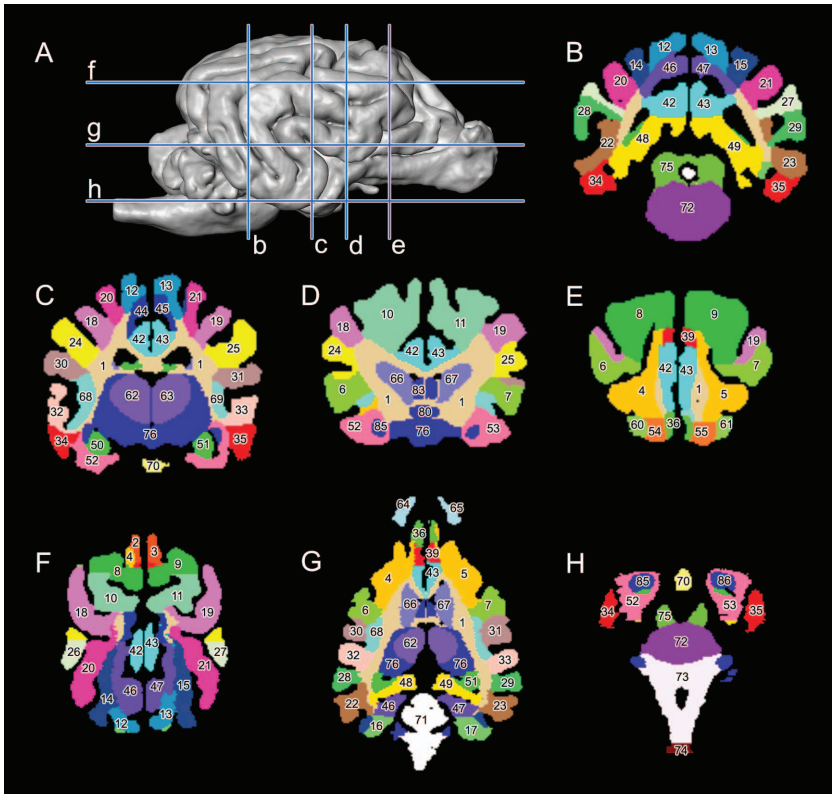

Fig. 5. The individual label map on different levels on sample images (for reference of the numbers see Table 1). Same letters (with upper and lower case) show the same level of section. (A) Three-dimensional model of the brain, right lateral view. (B–E) Transverse plane. (F–H) Dorsal plane

fitting on the average. This also means that, as the labels follow the surface contour of a single brain, within the grooves (sulci), a zero value is given; therefore, whenever the center of an fMRI activity is found inside a sulcus, the placement has to be assessed individually taking into account the adjacent gyri.

At present, in the literature, there are different descriptions of the canine brain areas regarding their names, placement, and boundaries. As a consequence, despite the fact that the placement of the gyri in our individual-based label map was determined according to the major anatomy textbooks (Constantinescu & Schaller, 2011; Evans & de Lahunta, 2012; Nickel et al., 2003; Singh, 2017; Uemura, 2015), the lack of clear definitions regarding the end of a gyrus resulted in subjective markings. Furthermore, nomenclature of the sulci and gyri is not consistently used across the different textbooks and atlases. For example, the gyrus suprasylvius (Evans & de Lahunta, 2012) is referred to as gyrus ectomarginalis or gyrus ectosagittalis elsewhere (Constantinescu & Schaller, 2011), the gyrus postcruciatus (Constantinescu & Schaller, 2011; Evans & de Lahunta, 2012; Nickel et al., 2003) is referred as gyrus sygmoideus posterior (Adrianov & Mering, 2010; Palazzi, 2011), or the gyrus marginalis (Evans & de Lahunta, 2012; Nickel et al., 2003) is referred as gyrus lateralis (Palazzi, 2011), and this is an additional reason for inconsistencies. Finally, our individual-based label map contains no lobar distinctions. In fact, only gyri are highlighted because different textbooks define the main lobes of the brain differently. For example, some include the postcruciate gyrus into the frontal lobe (Thomson & Hahn, 2012; Uemura, 2015) and others do not (Constantinescu & Schaller, 2011; Nickel et al., 2003; Schmidt & Kramer, 2015; Singh, 2017), and there is also a difference in how long the occipital lobe is described to extend toward the rostral and ventral direction (Nickel et al., 2003; Singh, 2017; Thomson & Hahn, 2012; Uemura, 2015); thus, the parieto-occipital and the temporo-occipital boundaries are also not well identified.

In contrast to human brains, dog brains highly differ in relation to the head shape (brachy-, mesati-, or dolichocephalic type). At present, this diversity is only considered by one study (Milne et al., 2016) but their brain templates contain only a few selected structures (brain as a whole, hippocampal formation, caudate nuclei, ventricular system) and the templates are not publicly available. Several neuroimaging software packages (e.g., SPM, FSL, BrainVoyager, 3D Slicer, MRIcron) contain an algorithm, which automatically extracts the data about the scanned brain, while normalizing it to a template brain. Later, the analysis can then run based on a label map linked to the template. To this date, when one needs to perform a reliable analysis on a dog brain, extraction is advised to be made in a manual way, which requires solid neuroanatomical background knowledge. The study by Milne et al. (2016) concluded that, for dogs, manual brain extraction and the use of brain shape-specific templates are more accurate compared to automatic brain extraction and application of a brain shape-specific template or to manual brain extraction and application of an average-based template. In fact, reliable automatic algorithms are not yet

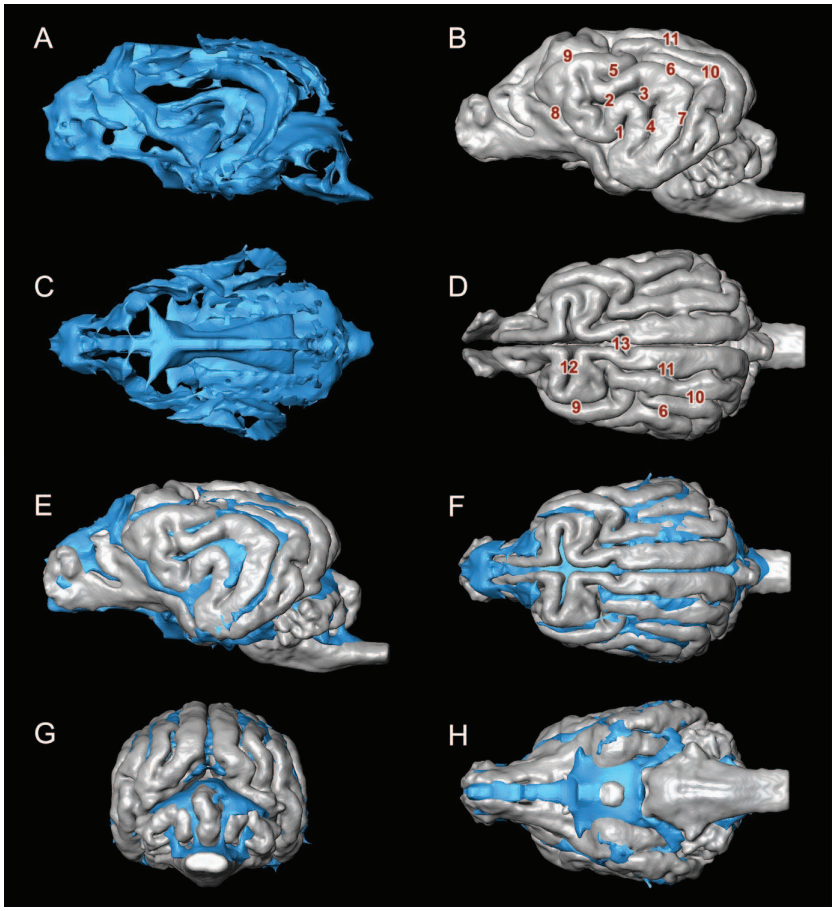

Fig. 6. Comparing the surface models of the average-based brain template (with blue), with the individual template brain (with gray). Separate (A–D) and co-registered (E–H) three-dimensional models are presented to show the localization of the sulci. (A, B, E) Left lateral view. (C, D, F) Dorsal view. (G) Caudal view. (H) Ventral view. (1) Fissura pseudosylvia. (2) Sulcus ectosylvius rostralis. (3) Sulcus ectosylvius medius. (4) Sulcus ectosylvius caudalis. (5) Sulcus suprasylvius rostralis. (6) Sulcus suprasylvius medius. (7) Sulcus suprasylvius caudalis. (8) Sulcus presylvius. (9) Sulcus coronalis. (10) Sulcus ectomarginalis. (11) Sulcus marginalis. (12) Sulcus cruciatus. (13) Fissura longitudinalis cerebri

available. Clearly, there is a need for deep learning algorithms (Akkus et al., 2017) for brain shape-specific templates, which will automatize this step for canine studies too, in addition to the automatic normalization of an individual brain to a selected template. Intracranial disorders or age-related alterations, like cortical or medullary atrophy or ventricular enlargement, should be also considered during analysis, as clinically healthy dogs may have marked ventriculomegaly. The normalization of these affected dogs to a template would mean that the outer cortical structures remain in place; however, the corpus callosum, cingulate gyrus, and the centrum semiovale will be dislocated depending on the extension of the lateral ventricles. This means that either dogs with anatomical abnormalities, such as considerable ventriculomegaly, will be excluded from neuroscientific studies or specific brain templates representing that different stages of symmetrical or asymmetrical ventricular enlargement are necessary in order to obtain an unbiased result at the end of the assessment. As a conclusion, it could be said that a common base for marking and referring to a given cortical structure and location of the canine brain would be highly advantageous, and this could be achieved by reaching an agreement on the nomenclature and definition of the borders between gyri and lobes.

CONCLUSION FOR FUTURE BIOLOGY

In this paper, we presented the most detailed dog brain label map to date, which was designed to aid neuroimaging analyses. Using the dog as a good translational model for human research is getting more widely accepted (Andics & Miklósi, 2018; Andics et al., 2014; Bunford et al., 2017; Cotman & Head, 2008; Head, 2013; Khanna et al., 2006; Wu et al., 2004). For example, the canine cognitive dysfunction syndrome (Landsberg et al., 2012, 2017; Madari et al., 2015) has some characteristics that are analogous to the early stages of the human Alzheimer's disease, which makes the dogs a promising model to study this disease more comprehensively. It is to be expected that the role of dogs in comparative research will keep growing in the future, and the need for accurate brain atlases and MRI templates will also increase. In our opinion, the template and label map described in this study will promote comparability of anatomical works between laboratories, as well as

between an exponentially increasing number of canine neuroscientific findings. Therefore, this work will significantly support fields such as social and cognitive neuroscience and diagnostic imaging.

Acknowledgments: The authors would like to thank the owners of the dogs who participated in the fMRI scannings; Márta Gácsi, Rita Báji, and Bernadett Miklósi for training the dogs; Anna Gábor and Dóra Szabó for running the MRI scans; and Patrizia Piotti for language proofing the manuscript.

Ethical Statement: All husbandry and experimental procedures have been approved by the institutional animal care and ethics committee and by the Government Office of Pest County Directorate of Food Chain Safety and Animal Health (XIV-I-001/520-4/2012) and conducted in accordance with relevant guidelines and regulations.

Funding Statement: This project has received funding from the European Research Council (ERC) under the European Union's Horizon 2020 research and innovation programme (grant agreement no. 680040), from the Hungarian Academy of Sciences via a grant to the MTA-ELTE 'Lendület' Neuroethology of Communication Research Group (grant no. LP2017-13/2017), the János Bolyai Research Scholarship of the Hungarian Academy of Sciences for EK and AA, the ÚNKP-18-4 New National Excellence Program of the Ministry of Human Capacities for EK, and Hungarian Brain Research Program 2017-1.2.1-NKP-2017-00002 for CK and EK.

Data Accessibility: Associated NIfTI and lut files can be accessed on FigShare: https://figshare.com/s/628cbf7d4210271ffe70. The lut files should be put into the "lut" folder of MRIcron if that program is used. After reopening the program, these new color files could be selected in the drop-down list of the main window. Label values are represented together with its coordinates in the main window.

Competing Interests: The authors declare no competing interests.

Authors' Contributions: KC offered significant contributions to the conceptualization, design, analysis of data; interpretation of the results; participation in the drafting; or revising the article. AA, ÖP, and EK participated in the drafting or revising the article.

REFERENCES

Adams, B., Chan, A., Callahan, H., Milgram, N. W. (2000) The canine as a model of human cognitive aging: recent developments. *Prog. Neuropsychopharmacol. Biol. Psychiatry 24*, 675–692.

Adluru, N., Zhang, H., Fox, A. S., Shelton, S. E., Ennis, C. M., Bartosic, A. M., Oler, J. A., Tromp do, P. M., Zakszewski, E., Gee, J. C., Kalin, N. H., Alexander, A. L. (2012) A diffusion tensor brain template for Rhesus Macaques. *NeuroImage 59*, 306–318.

Adrianov, O. S., Mering, T. A. (2010) *Atlas of the Canine Brain*. 1st ed. NPP Books, Arlington, MA.

Akkus, Z., Galimzianova, A., Hoogi, A., Rubin, D. L., Erickson, B. J. (2017) Deep learning for brain MRI segmentation: state of the art and future directions. *J. Digit. Imaging 30*, 449–459.

Andics, A., Gábor, A., Gácsi, M., Faragó, T., Szabó, D., Miklósi, Á. (2016) Neural mechanisms for lexical processing in dogs. *Science 353*, 1030–1032.

Andics, A., Gácsi, M., Faragó, T., Kis, A., Miklósi, A. (2014) Voice-sensitive regions in the dog and human brain are revealed by comparative fMRI. *Curr. Biol. 24*, 574–578.

Andics, A, Miklósi, Á. (2018) Neural processes of vocal social perception: dog-human comparative fMRI studies. *Neurosci. Biobehav. Rev. 85*, 54–64.

Berns, G. S., Brooks, A. M., Spivak, M. (2012) Functional MRI in awake unrestrained dogs. *PLoS One 7*, e38027.

Böttcher, P., Maierl, J., Schiemann, T., Glaser, C., Weller, R., Hoehne, K. H., Reiser, M., Liebich, H. G. (1999) The visible animal project: a three-dimensional, digital database for high quality three-dimensional reconstructions. *Vet. Radiol. Ultrasound 40*, 611–616.

Bunford, N., Andics, A., Kis, A., Miklósi, Á., Gácsi, M. (2017) *Canis familiaris* as a model for non-invasive comparative neuroscience. *Trends Neurosci. 40*, 438–452.

Carreira, L. M., Ferreira, A. (2015a) Anatomical variations in the pseudosylvian fissure morphology of brachy-, dolicho-, and mesaticephalic dogs. *Anat Rec. 298*, 1255–1260.

Carreira, L. M., Ferreira, A. (2015b) Longitudinal cerebral fissure anatomy variations in brachy-, dolicho- and mesaticephalic dogs and their importance to brain surgery. *Anat Rec. 298*, 1612–1621.

Constantinescu, G., Schaller, O. (2011) *Illustrated Veterinary Anatomical Nomenclature*. 3 rev. Thieme, Stuttgart.

Cook, P. F., Brooks, A., Spivak, M., Berns, G. S. (2015) Regional brain activity in awake unrestrained dogs. *J. Vet. Behav. 10*, 440.

Cotman, C. W., Head, E. (2008) The canine (dog) model of human aging and disease: dietary, environmental and immunotherapy approaches. *J. Alzheimers Dis. 15*, 685–707.

Cox, D. D., Savoy, R. L. (2003) Functional magnetic resonance imaging (fMRI) "brain reading": detecting and classifying distributed patterns of fMRI activity in human visual cortex. *NeuroImage 19*, 261–270.

Cuaya, L. V., Hernández-Pérez, R., Concha, L. (2016) Our faces in the dog's brain: functional imaging reveals temporal cortex activation during perception of human faces. *PLoS One 11*, e0149431.

Czeibert, K., Baksa, G., Grimm, A., Nagy, S. A., Kubinyi, E., Petneházy, Ö. (2019) MRI, CT and high resolution macroanatomical images with cryosectioning of a Beagle brain: creating the base of a multimodal imaging atlas. *PLoS One 14*, e0213458.

Datta, R., Lee, J., Duda, J., Avants, B. B., Vite, C. H., Tseng, B., Gee, J. C., Aguirre, G. D., Aguirre, G. K. (2012) A digital atlas of the dog brain. *PLoS One 7*, e52140.

Ella, A., Keller, M. (2015) Construction of an MRI 3D high resolution sheep brain template. *Magn. Reson. Imaging 33*, 1329–1337.

Evans, H. E., de Lahunta, A. (2012) *Miller's Anatomy of the Dog*. 4th ed. Saunders, St. Louis, MI.

Head, E. (2013) A canine model of human aging and Alzheimer's disease. *Biochim. Biophys. Acta 1832*, 1384–1389.

Hikishima, K., Quallo, M. M., Komaki, Y., Yamada, M., Kawai, K., Momoshima, S., Okano, H. J., Sasaki, E., Tamaoki, N., Lemon, R. N., Iriki, A., Okano, H. (2011) Population-averaged standard template brain atlas for the common marmoset (*Callithrix jacchus*). *NeuroImage 54*, 2741–2749.

Hussein, A. K., Sullivan, M., Penderis, J. (2012) Effect of brachycephalic, mesaticephalic, and dolichocephalic head conformations on olfactory bulb angle and orientation in dogs as determined by use of in vivo magnetic resonance imaging. *Am. J. Vet. Res. 73*, 946–951.

Kawamura, K., Naito, J. (1978) Variations of the dog cerebral sulci, compared in particular with those of the cat. *J Hirnforsch. 19*, 457–467.

Khanna, C., Lindblad-Toh, K., Vail, D., London, C., Bergman, P., Barber, L., Breen, M., Kitchell, B., McNeil, E., Modiano, J. F., Niemi, S., Comstock, K. E., Ostrander, E., Westmoreland, S., Withrow, S. (2006) The dog as a cancer model. *Nat. Biotechnol. 24*, 1065–1066.

Landsberg, G., Ma ari, A., Žilka, N. (eds.). (2017) *Canine and Feline Dementia: Molecular Basis, Diagnostics and Therapy*. Springer International Publishing.

Landsberg, G. M., Nichol, J., Araujo, J. A. (2012) Cognitive dysfunction syndrome: a disease of canine and feline brain aging. *Vet. Clin. North Am. Small Anim. Pract. 42*, 749–768.

Logothetis, N. K., Pfeuffer, J. (2004) On the nature of the BOLD fMRI contrast mechanism. *Magn. Reson. Imaging 22*, 1517–1531.

Madari, A., Farbakova, J., Katina, S., Smolek, T., Novak, P., Weissova, T., Novak, M., Zilka, N. (2015) Assessment of severity and progression of canine cognitive dysfunction syndrome using the CAnine DEmentia Scale (CADES). *Appl. Anim. Behav. Sci. 171*, 138–145.

Milne, ME, Steward, C, Firestone, SM, Long, S. N., O'Brien, T. J., Moffat, B. A. (2016) Development of representative magnetic resonance imaging-based atlases of the canine brain and evaluation of three methods for atlas-based segmentation. *Am. J. Vet. Res. 77*, 395–403.

Muñoz-Moreno, E., Arbat-Plana, A., Batalle, D., Soria, G., Illa, M., Prats-Galino, A., Eixarch, E., Gratacos, E. (2013) A magnetic resonance image based atlas of the rabbit brain for automatic parcellation. *PLoS One 8*, e67418.

Nickel, R., Schummer, A., Seiferle, E. (2003) *Lehrbuch der Anatomie der Haustiere, Band IV: Nervensystem, Sinnesorgane, Endokrine Drüsen, 4 unveränderte*. Enke, Berlin.

Nie, B., Chen, K., Zhao, S., Liu, J., Gu, X., Yao, Q., Hui, J., Zhang, Z., Teng, G., Zhao, C., Shan, B. (2013) A rat brain MRI template with digital stereotaxic atlas of fine anatomical delineations in paxinos space and its automated application in voxel-wise analysis. *Hum. Brain Map. 34*, 1306–1318.

Nitzsche, B., Boltze, J., Ludewig, E., Flegel, T., Schmidt, M. J., Seeger, J., Barthel, H., Brooks, O. W., Gounis, M. J., Stoffel, M. H., Schulze, S. (2018) A stereotaxic breed-averaged, symmetric T2w canine brain atlas including detailed morphological and volumetrical data sets. *Neuroimage 187*, 93–103.

Nitzsche, B., Frey, S., Collins, L. D., Seeger, J., Lobsien, D., Dreyer, A., Kirsten, H., Stoffel, M. H., Fonov, V. S., Boltze, J. (2015) A stereotaxic, population-averaged T1w ovine brain atlas including cerebral morphology and tissue volumes. *Front. Neuroanat. 9*, 69.

Palazzi, X. (2011) *The Beagle Brain in Stereotaxic Coordinates*. 1st ed. Springer New York, New York, NY.

Park, H. S., Shin, D. S., Cho, D. H., Jung, Y. W., Park, J. S. (2014) Improved sectioned images and surface models of the whole dog body. *Ann. Anat. 196*, 352–359.

Reveley, C, Gruslys, A, Ye, FQ, Glen, D., Samaha, J., Russ, B., Saad, Z., Seth, A., Leopold, D. A., Saleem, K. S. (2017) Three-dimensional digital template atlas of the macaque brain. *Cereb Cortex 27*, 4463–4477.

Rohlfing, T., Kroenke, C. D., Sullivan, E. V., Dubach, M. F., Bowden, D. M., Grant, K. A., Pfefferbaum, A. (2012) The INIA19 template and neuromaps atlas for primate brain image parcellation and spatial normalization. *Front Neuroinform 6*, 27.

Schmidt, M. J., Kramer, M. (2015) *MRT-Atlas ZNS-Befunde bei Hund und Katze* [MRI atlas and CNS findings in dogs and cats]. 1st ed. Enke, Stuttgart.

Schwarz, A. J., Danckaert, A., Reese, T., Gozzi, A., Paxinos, G., Watson, C., Merlo-Pich, E. V., Bifone, A. (2006) A stereotaxic MRI template set for the rat brain with tissue class distribution maps and co-registered anatomical atlas: application to pharmacological MRI. *NeuroImage 32*, 538–550.

Seidlitz, J., Sponheim, C., Glen, D., Ye, F. Q., Saleem, K. S., Leopold, D. A., Ungerleider, L., Messinger, A. (2018) A population MRI brain template and analysis tools for the macaque. *NeuroImage 170*, 121–131.

Singer, M. (1962) *The Brain of the Dog in Section*. Saunders, Philadelphia, PA.

Singh, B. (2017) *Dyce, Sack, and Wensing's Textbook of Veterinary Anatomy*. 5th ed. Saunders, St. Louis, MO.

Su, M., Head, E., Brooks, W. M., Wang, Z., Muggenburg, B. A., Adam, G. E., Sutherland, R., Cotman, C. W., Nalcioglu, O. (1998) Magnetic resonance imaging of anatomic and vascular characteristics in a canine model of human aging. *Neurobiol. Aging 19*, 479–485.

Tapp, P. D., Head, K., Head, E., Milgram, N. W., Muggenburg, B. A., Su, M. Y. (2006) Application of an automated voxel-based morphometry technique to assess regional gray and white matter brain atrophy in a canine model of aging. *NeuroImage 29*, 234–244.

Thompkins, A. M., Deshpande, G., Waggoner, P., Katz, J. S. (2016) Functional magnetic resonance imaging of the domestic dog: research, methodology, and conceptual issues. *Comp. Cogn. Behav. Rev. 11*, 63–82.

Thomson, C. E., Hahn, C. (2012) *Veterinary Neuroanatomy: A Clinical Approach*. 1st ed. Saunders W.B., Edinburgh/ Philadelphia.

Tóth, L., Gácsi, M., Miklósi, Á., Bogner, P., Repa, I. (2009) Awake dog brain magnetic resonance imaging. *J. Vet. Behav. 4*, 50.

Uemura, E. E. (2015) *Fundamentals of Canine Neuroanatomy and Neurophysiology*. 1st ed. Wiley-Blackwell, Ames, Iowa.

Ulmer, S., Jansen, O. (eds.). (2013) *fMRI: Basics and Clinical Applications*. 2nd ed. Springer, New York, NY.

Wu, Y., Loper, A., Landis, E., Hettrick, L., Novak, L., Lynn, K., Chen, C., Thompson, K., Higgins, R., Batra, U., Shelukar, S., Kwei, G., Storey, D. (2004) The role of biopharmaceutics in the development of a clinical nanoparticle formulation of MK-0869: a beagle dog model predicts improved bioavailability and diminished food effect on absorption in human. *Int. J. Pharm. 285*, 135–146.